Renewable Energy 256 (2026) 124632

Contents lists available at ScienceDirect

Renewable Energy

journal homepage: www.elsevier.com/locate/renene

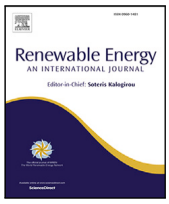

Modelling and optimal control of tidal barrages: A moment-based approach

Agustina Skiarski [a,*], Nicolás Faedo [b], John V. Ringwood [a]

[a] Centre for Ocean Energy Research, Department of Electronic Engineering, Maynooth University, Maynooth, Co. Kildare, Ireland
[b] Marine Offshore Renewable Energy Lab, Department of Mechanical and Aerospace Engineering, Politecnico di Torino, Torino, Italy

ARTICLE INFO

Keywords:
Tidal barrages
Optimal control
Moment-based control
Tidal energy
Artificial Neural Networks

ABSTRACT

Tidal barrages generate electrical energy using the tidal height variations throughout the day, and stand out from other renewable energy schemes because of their inherent storage capabilities and the relatively slow variation of the tides, allowing flexibility in their operation. The resulting optimal control problem of operating tidal barrages has unique features that call for a range of possible operating modes (generating, sluicing and pumping). This paper presents a comprehensive model for tidal barrage power plants, using the La Rance power plant as case study. The operation of the hydraulic turbines is modelled using a generic hill chart, which accounts for all possible operating points (not only those with maximum efficiency, as commonly seen in the literature). An artificial neural network was designed and trained to obtain a compact function approximation for the hill chart. The optimal control problem is solved using moment-based control, a mathematical tool from the family of weighted residual methods, broadly applied in wave energy control. Moment-based control is implemented by parameterising the external and control inputs with a harmonic expansion, and the nature of the frequency range required for an efficient parameterisation is explored.

1. Introduction

Driven by the need to reduce CO_2 emissions, nations worldwide are transitioning towards renewable energy sources to generate electricity. As the penetration of renewables in power grids increases, new challenges arise for system operators, given the intermittent and unpredictable behaviour of renewable sources, such as wind and solar. Such issues suggest a need for new technologies that could complement wind and solar generation to bring stability to power grids, one example being energy storage facilities. A less explored option, but with significant potential, are tidal barrages, which use changes in the tidal elevation throughout the day to generate electricity.

Tidal barrages consist of an embankment located in a coastal area that separates the sea from a basin, with turbines and sluice gates that allow the passage of water between the basin and the open sea, as seen in Fig. 1. As the tidal elevation increases and decreases, the head difference created between the sea and the inner basin level is used to fill and empty the basin through the turbines, thus generating electricity. Fig. 2 shows an example of the operation of a tidal barrage in time. In addition to the basic generation modes, pumping and sluicing can be added to enhance the generating capacity of the tidal barrage, whereby a desired operating head can be reached. As a result, there are several possible ways to operate the turbines and sluice gates in the barrage, with flexibility over the duration and timing for each stage. The energy available for generation will not only depend on the resource (*i.e.* the tidal elevation), but also on the dimensions of the basin and the capacity of the turbines and sluice gates, *i.e.* how fast the basin can be filled or emptied. Furthermore, the operation during one generating cycle determines the available head on the following cycles, also influencing how much energy can be harnessed in the next stages. Finding the optimal operation of the barrage for a given objective (for instance, energy maximisation) is therefore non-trivial, and involves a large number of variables.

The literature on control of tidal barrages typically focuses on two approaches: Fixed parameter optimisation and flexible operation optimisation. In fixed parameter optimisation, the parameters that define each operational phase of the barrage are predefined based on a preliminary optimisation analysis and then used to simulate the system. Examples of fixed parameter optimisation are [1], where different starting heads (*i.e.* the head that triggers generation) are evaluated *a priori* to determine which is the optimal, or [2], where the optimal timing of generation periods is computed via an analytic model. Flexible operation optimisation (as presented in this study) involves selecting each operating stage dynamically using an optimisation routine, which can account for the variations in tidal range throughout the month, and can handle more complex tidal barrage models, achieving better solutions compared to fixed parameter optimisation.

* Corresponding author.
E-mail address: agustina.skiarski.2024@mumail.ie (A. Skiarski).

https://doi.org/10.1016/j.renene.2025.124632
Received 20 June 2024; Received in revised form 13 October 2025; Accepted 14 October 2025
Available online 21 October 2025
0960-1481/© 2025 Published by Elsevier Ltd.

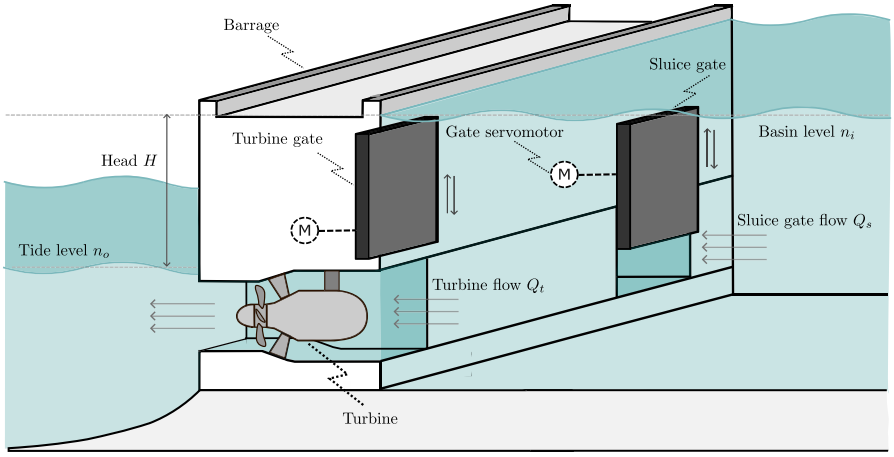

Fig. 1. Diagram of a tidal barrage power plant: an embankment with turbines and sluice gates separates the open sea from a basin. The water flows in and out of the basin through the turbines and sluice gates.

Flexible operation optimisation can be local, by exploiting relatively standard discretisation techniques (*i.e.* MPC-like approaches [3]), or globally, by considering a global parameterisation of the evolution of the tidal elevation during a time window [4]. For instance, a local discretisation approach exploited in the literature is based on establishing a sequence of barrage operating modes (generating, pumping and sluicing) and optimising the duration [5] or starting head [6] of each mode throughout each semi-diurnal tidal cycle independently. The method can be improved by further incorporating the subsequent tidal cycle as well ([7] using the duration of operational modes and [8] using head), evidencing the influence of barrage operation on the energy generation of subsequent cycles. The underlying assumptions, within such a local framework, automatically imply that there is no overlap between turbine and sluice gate operation, and the turbine flow is uniquely determined by the operating head, which constrains the solution space. In [9], the control action is defined in terms of the operational modes and the turbine speed, and the sluice gates are operated independently. Although the study in [9] also considers a predefined sequence of operational modes, it shows that operating the sluice gates simultaneously with the turbines achieves higher energy output than only sluicing when the turbines are inactive.

Studies on tidal barrage control often use sophisticated genetic [8] and evolutionary algorithms [9] to handle all possible combinations within a large (discretised) design space. On the other hand, in [10], the continuous-time formulation of tidal barrage operation is solved by using a discretisation based on *moments*. In moment-based analysis, a technique originally developed for model reduction [11] and broadly applied to solve the energy-maximising control problem in wave energy conversion [12], a set of basis functions is used to parameterise the inputs (both external and manipulated) and compute the steady state response of the system, similarly to spectral weighted residual methods [13]. The moment-based control framework applied to tidal barrages, presented in [10] and extended to incorporate model enhancements in [4], is used to manipulate turbine and sluice gate flow, resulting in more flexible operation of the barrage (in terms of the timing of each operational mode). However, both [4,10] consider monochromatic input tides, neglecting the variation in tidal range throughout spring-neap cycles. Furthermore, [4] operates based on a simplified turbine model, which can lead to non-representative control solutions (*i.e.* turbine flow and sluice gates operation); without a tailored turbine representation, able to represent accurately (yet computationally efficient) effective power flow conversion, the moment-based controller can compute turbine profiles which do not take into account losses accordingly, leading to suboptimal results in realistic operations. To represent the turbines realistically, the complete hill chart of the turbines, which constitutes a non-linear mapping determining turbine efficiency at each operating point, must be considered within the optimisation framework. Nonetheless, a direct consideration of the hill chart within the corresponding optimisation procedure, accounting for all operating conditions, can considerably increase the complexity and computational burden of the control problem, rendering the optimisation procedure intractable.

In this paper, a comprehensive tidal barrage model is presented, including all main components relevant for its operational optimisation, using the La Rance power plant as a case study. The focus is on the hydraulic turbines, which are modelled using a neural-network-based structure as a function approximation of the turbines' hill chart. The operation of the turbines includes pumping under positive head scenarios, which is seen in the operation of the turbines from La Rance [14], yet is neglected in the research literature. Applying the control action over both the turbine and sluice gate flows, without a pre-defined operational sequence, avoids predetermination of operational modes, enabling overlapping of sluicing mode with generating or pumping modes, leading to an overall improved performance of the controller. Moment-based control is then used to solve the energy-maximising optimal control problem, and the performance of the controller is assessed in terms of its relevant design parameters. Previous work on moment-based control of tidal barrages [4] use a simplified turbine model, and evaluates the controller over a short time window, using a monochromatic input tide. In contrast, the novelty of the work presented in this paper relies on two main aspects:

- Integrating a turbine model, that accounts for the complete operational range of the tidal barrage, within the moment-based control framework;
- Developing a formulation of the tidal barrage optimal control problem in the moment-domain that incorporates a polychromatic representation of the tidal elevation, thus accounting for variations in tidal range throughout spring-neap cycles.

The remainder of this paper is structured as follows. Section 2 describes the models developed for each component of the tidal barrage. Section 3 describes the theory behind the moment-based framework and its implementation for solving the tidal barrage energy-maximising optimal control problem. Section 4 presents the study case of the La Rance power plant, the results of the solution of the energy-maximising optimal control problem, and a harmonic analysis to refine the relevant discretisation that should be used to parameterise the inputs of the system. Finally, Section 5 outlines the conclusions of this paper.

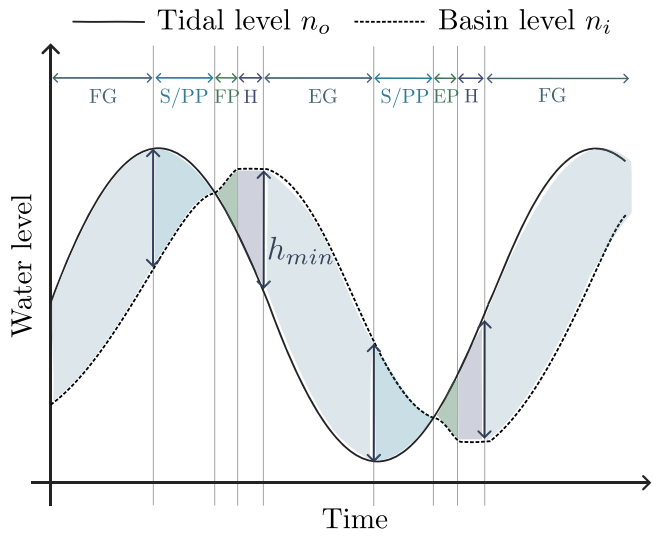

Fig. 2. Example of the operation of a tidal barrage in time, described in Section 2.1.

2. Tidal barrage model

2.1. Operating modes

Here, the basic principles behind the operation of tidal barrages are described, including two-way generation with pumping, illustrated in Fig. 2. Two-way generation refers to the capability of the turbines to generate both on ebb (while emptying the basin) and on flood (while filling the basin).

When the tide level n_o (bold line in Fig. 2) is higher than the basin level n_i (dotted line), the potential energy created by the head between the basin and the sea drives the water flow into the basin through the turbines, generating electricity while raising the basin level n_i. This operational mode is called flood generation (FG). During this stage, the sluice gates can be opened, increasing the water flow through the barrage, or closed. After a certain minimum head h_{min} is reached, the water pressure is insufficient for the turbines to generate hydraulic power, so the water flows freely through the sluice gates and/or turbine ducts, known as sluicing mode (S). During this stage, the turbines may also operate as pumps, increasing the flow and filling the basin faster. In this paper, this type of operation is referred to as positive pumping (PP), where the turbine operates as a pump aided by gravity. After the water levels inside and outside the basin are equal, the turbines can pump the water into the basin *against gravity* to increase the available head, termed flood pumping (FP). The inner level is then held (H) until the tidal elevation decreases to an extent that the minimum head is reached, allowing the turbines to generate again, this time by emptying the basin and entering ebb generation mode (EG). When the minimum head is again reached, the basin is emptied using the sluice gates and/or turbine ducts (S), or by positive pumping (PP). Then, the turbines can pump the water out of the basin by ebb pumping (EP) and, afterwards, the basin level is held (H), and the cycle repeats. Note that operating the turbines as pumps means injecting energy into the system, rather than generating, but with an increase in the available potential energy afterwards [15], giving an overall greater positive generated energy.

2.2. Standing assumptions

Within this section, the basic standing assumptions adopted in this study to develop the tidal barrage model are summarised. Firstly, the dominant dynamics of the system are given by the slow variation of the tidal elevation (*slow* refers to a variation with a time span of minutes/hours). That implies that the dominant hydrodynamic processes relevant to the operation of the barrage are those given by the principle of mass conservation:

$$\frac{\mathrm{d}n_i}{\mathrm{d}t} = \frac{-Q_t - Q_s}{A_b(n_i)}, \tag{1}$$

also known as the 0D hydrodynamic model [16]. In Eq. (1), $n_i(t)$ is the inner basin water level, $Q_t(t)$ and $Q_s(t)$ are the flows through the turbines and sluice gates, respectively, and $A_b(n_i)$ is the basin area, which is a function of the basin level, as described in Section 2.6.

Moreover, since the overall main dynamics of the system are slow, the dynamic response of the turbine, electrical generator, and sluice gates, which are orders of magnitude faster, can be omitted for operational optimisation. The electrical power output is assumed to be equal to the mechanical power of the turbine P_t. Lastly, all the turbines in the barrage are assumed to operate in unison, that is, the turbines are not controlled individually, but as a single unit. The same applies to the sluice gates.

2.3. Tidal elevation

The tidal elevation can be described as the sum of constituents [17]:

$$n_o(t) = \sum_{i=1}^{N_i} A_i \cos(\omega_i t - \phi_i), \tag{2}$$

where $N_i \in \mathbb{N}/0$ is the number of constituents considered. Each constituent i has a certain period T_i, with $T_i/T_j \in \mathbb{Q}$, $\forall i \neq j$, corresponding to a frequency $\omega_i = 2\pi/T_i$, that depends on the particular phenomenon that causes each specific constituent, and a certain amplitude A_i (in meters) and phase ϕ_i that depends on the location of the tidal height measurement point on Earth.

Eq. (2) implies that the tidal elevation is periodic, with consecutive rises and falls in sea water level. In this study, the term *tidal cycle* refers to the time interval in which there is one peak and one trough in the water level. That is, during one tidal cycle, the basin in the barrage is filled once and emptied once.

2.4. Turbine model

The bulb turbine, which is the type of turbine used in the La Rance power plant, is the most commonly used turbine type in tidal barrages [18]. The operation of these turbines can be split into five distinct modes, listed in the following:

- Ebb generation (EG),
- ebb pumping (EP),
- flood generation (FG),
- flood pumping (FP),
- idling, and
- positive pumping (PP).

Generation and pumping are differentiated for ebb and flood since, in general, the guide vanes in the turbine shaft are unidirectional, meaning that the flow can be controlled more efficiently in one way compared to the other. As a result, the turbine efficiency is different for ebb and flood operational modes [19].

2.4.1. Operating points

The efficiency of a bulb turbine is given by a hill chart, which is a static mapping of the operation of the turbine created by the manufacturer. Hill charts have unitary speed n_{11} and unitary discharge Q_{11} as inputs so that they can be scaled to different turbine sizes, based on affinity laws [20]. Each level curve of the hill chart corresponds to a value of turbine efficiency so that the turbine power can be determined for every head-flow pair. As a result, instead of parameterising each

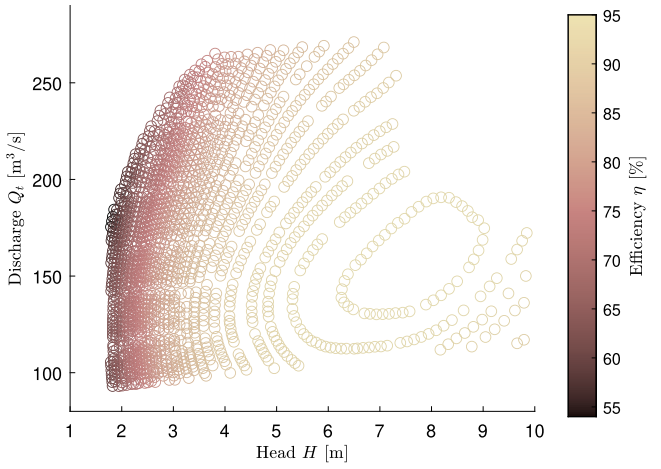

Fig. 3. Turbine efficiency, taken from the Andritz Hydro hill chart in [1].

operational mode of the turbine separately, the instantaneous head-flow pair is used to calculate the turbine efficiency and inform the controller whether the operation corresponds to ebb or flood generation or pumping. For this study, the hill chart from an Andritz Hydro turbine is digitised [1] and converted into a head-flow plot (with the head $H = n_i - n_o$ on the horizontal axis and the turbine flow Q_t on the vertical axis) using the parameters from the turbines in La Rance power plant, as seen in Fig. 3.

Since there is no analytical description of a hill chart, within this study, an artificial neural network (ANN) is trained to obtain a fitted function that can allow interpolation between known points. The use of an ANN has the purpose of defining, *offline*, a parametric form of the hill chart that can be then used within the controller, avoiding the need for interpolation at each iteration of the optimisation. The ANN is trained once, using the operating points of the turbine extracted from the digitised hill chart, and included in the model as a function $\eta(Q_t, H)$.

According to Cybenko's theorem [21], a multi-layer perceptron with one hidden layer can uniformly approximate any continuous function; hence, the chosen neural network consists of only one hidden layer. A maximum of 350 neurons is considered for the layer, giving 350 possible networks, each of them trained and tested with the mapping from Fig. 3. The performance of each neural network is assessed in terms of the mean squared error (MSE). The selected training algorithm is Levenberg–Marquardt back-propagation, given its relatively fast convergence [22]. Fig. 4(a) shows the resulting MSE on the training and test sets for each architecture. It can be seen that, while the MSE on the training set decreases monotonically with an increasing number of neurons, the MSE on the testing set reaches a minimum and then increases due to overfitting. The selected architecture is therefore a network with 115 neurons which, in this case, has the lowest MSE on the test data. Fig. 4(b) shows that there is a slight positive slope in the MSE for the test dataset after 2200 epochs, potentially indicating overfitting. The selected number of epochs used for training was 2500, which is considered enough to achieve low MSE in both training and testing sets without overfitting. Table 1 shows the parameters describing the chosen neural network, and Fig. 5 shows a schematic of its architecture.

In this study, the representation of turbine efficiency with an ANN aims to achieve a comprehensive, yet computationally feasible, representation of the turbines. If desired, the same ANN can be trained with the hill chart data from the actual turbines (in this case, the turbines from La Rance power plant), rather than using a generic hill chart data used in this paper, which was readily available to the authors.

Table 1
Parameters of the neural network characterising the turbine operating points mapping.

Inputs	Q_t, H
Output	η
No. of hidden layers	1
No. neurons in hidden layer	115
No. epochs	2500
No. datapoints	1598
Training set	70%
Testing set	30%
Activation function of hidden layers	Log-sigmoid
Activation function of output layer	Positive linear
Training algorithm	Levenberg–Marquardt
MSE (test data)	0.01

2.4.2. Turbine efficiency mapping

From the turbine characterisation in Section 2.4.1 the turbine efficiency for each pair (Q_t, H) can be determined. Efficiency is typically defined as the ratio between the power output P_{out} and power input P_{in} of a system, *i.e.*

$$\eta = \frac{P_{out}}{P_{in}}. \tag{3}$$

Generation takes place when the head $H = n_i - n_o$ has the same sign as the flow Q_t (in this study, the convention is that the flow leaving the basin is positive; that is, for ebb operation, $Q_t > 0$, and flood operation, $Q_t < 0$). During ebb generation, the power injected into the barrage system is the hydraulic power due to the hydraulic head (denoted as P_{hyd}), and the power output is the mechanical power generated by the turbine:

$$\eta_{\mathrm{EG}} = \frac{P_t}{P_{hyd}} = \frac{P_t}{\rho g H Q_t}, \tag{4}$$

where g is the gravitational constant, ρ is the sea water density, and the EG subscript refers to ebb generation, as per the nomenclature used in Fig. 2. During flood generation, the same definition applies, although with a decrease in efficiency. Usually, the peak efficiency is around 90% for ebb operation, and around 70% for flood operation [19]. Therefore, from now on, the efficiency during flood operation is assumed to be 20% lower than the efficiency during ebb operation, and the resulting efficiency during flood generation η_{FG} is

$$\eta_{\mathrm{FG}} = \frac{P_t}{P_{hyd}} = \frac{0.8 P_t}{\rho g H Q_t} = 0.8\,\eta_{\mathrm{EG}}. \tag{5}$$

Pumping, on the other hand, takes place when the sign of H is opposite to the sign of Q_t, meaning that the turbines are driving the water against the hydraulic head. The purpose of pumping in tidal barrages is to increase the operating head during the next tidal cycle, so that, by injecting power into the system for a certain time interval, the overall energy produced in a subsequent period increases. During ebb pumping, the input power comes from the electrical generator, which draws power from the grid, and the output hydraulic power pushes the water out of the basin. The efficiency during ebb pumping operation η_{EP} is

$$\eta_{\mathrm{EP}} = \frac{P_{hyd}}{P_t} = \frac{\rho g H Q_t}{P_t}. \tag{6}$$

In flood pumping, the same efficiency loss applies as during flood generation, *i.e.* the efficiency during flood pumping η_{FP} is calculated as:

$$\eta_{\mathrm{FP}} = \frac{P_{hyd}}{P_t} = \frac{0.8 \rho g H Q_t}{P_t} = 0.8\,\eta_{\mathrm{EP}}. \tag{7}$$

Bulb turbines need a minimum pressure difference, *i.e.* a minimum head h_{min}, to generate power. When the operating head is lower than h_{min}, the turbine gate could be closed, blocking the water flow through the turbine duct, or open, allowing the free passage of water without converting its potential energy into mechanical energy (known as idling

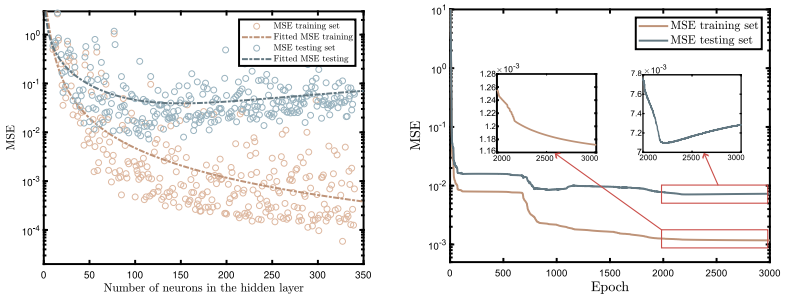

(a) The MSE on the training set is monotonically decreasing as the number of neurons increases, while the MSE on the testing set reaches a minimum and then increases.

(b) Variation in MSE with number of epochs for an ANN with a single layer of 115 neurons.

Fig. 4. Criteria for choosing the neural network architecture and the number of epochs used for training.

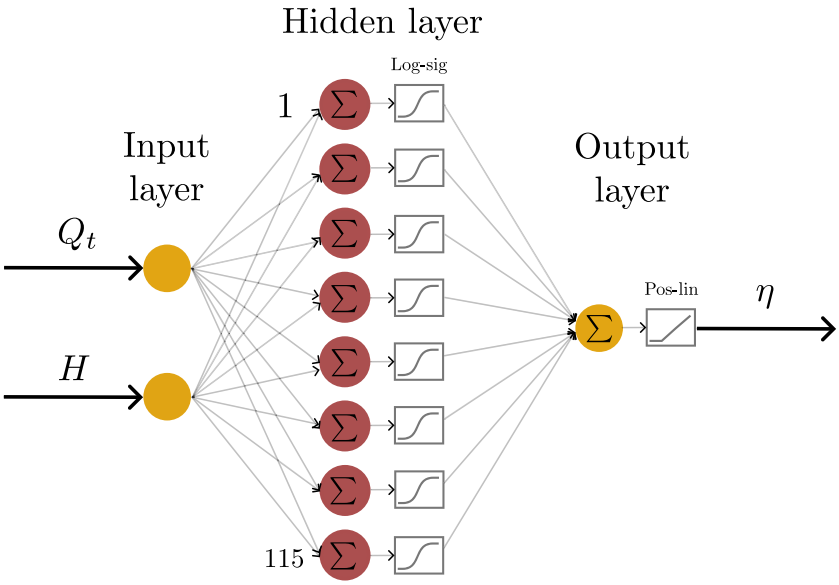

Fig. 5. Architecture of the neural network characterising the turbine operating points mapping.

mode). During idling mode, the water flow is given by the orifice equation:

$$Q_t = C_{dt} A_t \sqrt{2gH} \quad \text{with} \quad A_t \le A_{t_{max}} \tag{8}$$

where C_{dt} is the discharge coefficient of the turbine gate, $A_{t_{max}}$ is the maximum area of the turbine duct and A_t is the instantaneous turbine duct area, which can be manipulated with the turbine guide vanes. Given that there is no energy conversion during idling mode, the efficiency of the turbine is considered to be 0. Another option is that the turbine could pump the water in or out of the basin, aided by gravity, which here is referred to as positive pumping. If Q_t is greater than the orifice equation (considering maximum duct area):

$$Q_t > C_{dt} A_t \sqrt{2gH} \quad \text{with} \quad A_t = A_{t_{max}}, \tag{9}$$

the additional flow is being pumped. The equivalent positive pumping efficiency η_{PP} (since the energy consumed is being used only to pump the additional flow) is calculated as:

$$\eta_{\text{PP}} = \begin{cases} \eta_{\text{EP}} \left[1 - \dfrac{C_{dt} A_t \sqrt{2gH}}{Q_t} \right] & \text{if } Q_t > 0, \\ \eta_{\text{FP}} \left[1 - \dfrac{C_{dt} A_t \sqrt{2gH}}{Q_t} \right] & \text{if } Q_t < 0, \end{cases} \tag{10}$$

The following efficiency map for the turbine $\mu(Q_t, H) \in [0, 1]$ is used to formally incorporate the above description of the efficiency for each operating mode:

$$\mu : \begin{cases} \eta_{\text{EG}} & \text{if } \operatorname{sign}(Q_t) = \operatorname{sign}(H) > 0,\ H \ge h_{min}, \\ \eta_{\text{FG}} & \text{if } \operatorname{sign}(Q_t) = \operatorname{sign}(H) < 0,\ H < -h_{min}, \\ \dfrac{1}{\eta_{\text{EP}}} & \text{if } \operatorname{sign}(Q_t) \ne \operatorname{sign}(H),\ Q_t > 0, \\ \dfrac{1}{\eta_{\text{FP}}} & \text{if } \operatorname{sign}(Q_t) \ne \operatorname{sign}(H),\ Q_t < 0, \\ 0 & \text{if } |H| < h_{min},\ Q_t \le C_{dt} A_t \sqrt{2gH}, \\ \dfrac{1}{\eta_{\text{PP}}} & \text{if } |H| < h_{min},\ Q_t > C_{dt} A_t \sqrt{2gH}, \end{cases} \tag{11}$$

so that the power output from the turbine can be calculated as:

$$P_t = \mu(Q_t, H) \rho g Q_t H. \tag{12}$$

The ANN described in Section 2.4.1 is used to calculate η_{EG}, η_{FG}, η_{EP} and η_{FP} are calculated in terms of η (the output of the ANN):

$$\begin{aligned} &\eta_{\text{EG}} = \eta \ \text{(ebb generation)}, \\ &\eta_{\text{FG}} = 0.8\,\eta \ \text{(flood generation)}, \\ &\eta_{\text{EP}} = \eta \ \text{(ebb pumping)}, \\ &\eta_{\text{FP}} = 0.8\,\eta \ \text{(flood pumping)}, \end{aligned} \tag{13}$$

and η_{PP} is calculated as in Eq. (10).

The mapping μ in (11) is highly discontinuous and difficult to handle numerically. For ease of computation, the discrete jumps in the mapping are implemented as smooth transitions using hyperbolic tangent functions.

2.5. Sluice gates model

As mentioned in Section 2.2, the sluice gates are modelled taking into consideration only their quasi-static position (not the dynamic response of the servomotor that moves the sluice gates). The equation governing the flow through the sluice gates is the orifice equation, also used for the idling mode of operation in the turbines:

$$Q_s = C_{ds} A_s \sqrt{2gH}, \tag{14}$$

where C_{ds} is the discharge coefficient of the sluice gates and A_s is the sluice gates area. In essence, Eq. (14) shows that the flow through the sluice gates can be controlled by varying the sluice gate area.

2.6. Basin topology

Tidal barrages are located in estuaries or bays, and the topology of the basin is usually irregular, depending on the bathymetry of the site. Therefore, the impounded area inside the basin, A_b, varies with the basin water level n_i.

It is a common practice in the literature to approximate the function $A_b(n_i)$ in terms of a polynomial. In the present study, following the model from [14], the basin area A_b is approximated as a linear function of n_i.

3. Moment-based optimal control framework

Moment-based theory, originally developed as a model reduction tool, uses the mathematical concept of *moments* to characterise the steady-state behaviour of a (linear or non-linear) dynamical system. In particular, the main idea is to parameterise the steady-state behaviour of the tidal barrage system, driven by the tidal elevation n_0, in terms of the approximate solution of a corresponding invariance equation. Such a steady-state representation is then used to transcribe the infinite-dimensional optimal control problem associated with the optimal operation of the tidal barrage, leading to a finite-dimensional (tractable) nonlinear program able to provide policies for the operation of the turbines Q_t and sluice gates Q_s, via off-the-shelf standard numerical optimisation routines. Aiming to keep this paper reasonably self-contained, within this section, the basic formulation of an optimal control problem (OCP) using the moment-domain framework is introduced.

3.1. Moment-based theory

Let us consider a non-linear single-input single-output continuous-time dynamical system described, for $t \in \mathbb{R}^+$, by the set of equations

$$\begin{aligned} \dot{x} &= f(x,u), \\ y &= h(x), \end{aligned} \tag{15}$$

with $x(t) \in \mathbb{R}^n$, $u(t) \in \mathbb{R}$ and $y(t) \in \mathbb{R}$, and $f : \mathbb{R}^n \times \mathbb{R} \to \mathbb{R}^n$ and $h : \mathbb{R}^n \to \mathbb{R}$ the state transition and output mappings, respectively. Consider that the input u can be described in terms of the following exogenous system (commonly termed a signal generator):

$$\begin{aligned} \dot{\theta} &= S\theta, \\ u &= L\theta, \end{aligned} \tag{16}$$

where $\theta(t) \in \mathbb{R}^\nu$, $S \in \mathbb{R}^{\nu\times\nu}$ is a non-derogatory matrix defining the class of input signals generated by (16), and $L^\intercal \in \mathbb{R}^\nu$. The resulting interconnected system has the form of:

$$\begin{aligned} \dot{\theta} &= S\theta, \\ \dot{x} &= f(x, L\theta), \\ y &= h(x). \end{aligned} \tag{17}$$

Considering the assumption that the signal generator (16) is such that $\lambda(S) \subset \mathbb{C}^0$ with simple eigenvalues guarantees that (16) generates bounded trajectories and, therefore, adopting a set of mild assumptions, the definition of the non-linear moment of the system is well-posed. Another assumption is that the triple $(L, S, \theta(0))$ is minimal, *i.e.* it is observable and excitable. Then, there exists a mapping π defined by

$$\frac{\partial \pi(\theta)}{\partial \theta} S\theta = f(\pi(\theta), L\theta), \tag{18}$$

such that the *moment* of the system is $h \circ \pi = h(\pi)$. Note that, for any fixed trajectory $\theta(t)$, the steady-state output response of the system is $y^{ss}(t) = h(\pi(\theta(t)))$ [23].

While the invariance equation in (18) effectively provides a characterisation of the steady-state manifold of the interconnected system, *i.e.* a parameterisation of its steady-state behaviour in terms of the signal generator (16), computing an analytical solution for a generic set of system maps $\{f, h\}$ is not trivial. Following [13], where moment-based methods are shown to be strongly connected with the family of weighted residual methods (WRM) [13], a Galerkin-like approximation procedure is adopted within this paper, briefly described in the following.

Following a standard WRM procedure, given any fixed trajectory $\theta(t)$, the following ansatz for π, $\overline{\pi}$, is proposed:

$$\pi \approx \overline{\pi} = \overline{\Pi}\theta, \tag{19}$$

where $\overline{\Pi}^\intercal \in \mathbb{R}^\nu$. Subsequently, an error function, commonly called *residual*, is defined as:

$$\mathcal{R} := \overline{\Pi} S\theta - f(\overline{\Pi}\theta, L\theta). \tag{20}$$

To compute an approximate solution for Eq. (20), a finite set of *time collocation points* $N_c \in \mathbb{N}$ is chosen, *i.e.* the residual is projected onto a set of uniformly shifted Dirac-delta distributions $\{\delta(t - t_j) \equiv \delta_j\}_{j=1}^{N_c}$:

$$\int \mathcal{R}\delta_j \mathrm{d}t = \mathcal{R}(t_j) = 0, \tag{21}$$

for every $j \in \{1, \ldots, N_c\}$.

3.2. Optimal control problem of tidal barrage operation

The optimal control problem for tidal barrages consists of the following building blocks:

- An objective function f_o,
- an external input n_o (*i.e.* the tidal elevation),
- a set of manipulated variables, and
- a set of input and state constraints.

Given the flexibility of tidal barrages, different objective functions can be selected. This study focuses on energy maximisation over a given time interval $\Omega = [t_1, t_2] \subset \mathbb{R}^+$, with an additional term $C : \mathbb{R}^+ \to \mathbb{R}$ that penalises abrupt operation of the sluice gates [4]. The selected manipulated variables are Q_t and A_s, that is, the flow through the turbines and sluice gates, respectively. Inequality constraints, reflecting physical limitations in the system, are considered for Q_t, A_s, P_t and n_i, and a single state equality constraint, reflecting the system dynamics

(*i.e.* Equation (1)). The resulting OCP can be formalised as follows:

$$(Q_t^{\text{opt}}, A_s^{\text{opt}}) = \arg \max_{(Q_t, A_s)} \left[\int_\Omega P_t - C \, \mathrm{d}t \right],$$

subject to:

$$\begin{aligned} & A_b(n_i)\dot{n}_i = -Q_t - C_{ds} \, \text{sign}(n_i - n_o) \sqrt{2g \left| n_i - n_o \right|} A_s, \\ & n_i^{\min} \le n_i \le n_i^{\max} \qquad \text{(basin water level limits)}, \\ & |Q_t| \le Q_t^{\max} \qquad \text{(turbine flow limits)}, \\ & 0 \le A_s \le A_s^{\max} \qquad \text{(sluice gate opening limits)}, \\ & |P_t| \le P_t^{max} \qquad \text{(instantaneous power limits)}, \end{aligned} \tag{22}$$

where C is a continuous quadratic function over the interval $[0, A_s^{\max}] \subset \mathbb{R}^+$ representing the energy consumption of the sluice gates:

$$C = k_w \dot{A}_s^{\,2}, \tag{23}$$

with $k_w \in \mathbb{R}^+$ a non-dimensional weighting coefficient. The purpose of this penalty cost function is to account for the energy consumption of the servomotor of the sluice gates, so that they are not overutilised.

3.2.1. Representation of tidal elevation using moments

Given the harmonic nature of the tidal elevation, *i.e.* the external input of the tidal barrage system, it is reasonable to construct the signal generator used to parameterise the OCP (22) such that it generates a family of harmonic functions. Note that these harmonic functions must share the same fundamental frequency, otherwise the OCP is not necessarily well-posed (see [23]). On the other hand, the constituents used to model the tidal elevation do not necessarily share a fundamental frequency; in fact, that is not the case for the constituents that are most prominent in most areas of the globe.[1] Therefore, the tidal elevation described in Eq. (2) can be projected onto a space with a known fundamental frequency, providing a suitable (approximate) representation of the resource using the implicit form description (16).

The tidal elevation function n_o is now mapped onto a harmonic signal generator with state-vector θ in the moment domain, with fundamental frequency ω_o. The choice of ω_o, together with a cut-off frequency ω_{max}, determines the accuracy of the representation for n_o. Given that n_o is not necessarily periodic, following [24], n_o is windowed onto a mapping with period $T_o = 2\pi/\omega_o$, in accordance with the definition of the signal generator. Considering the interval $\Omega = [0, T_o] \subset \mathbb{R}^+$:

$$n_o^{\mathcal{L}} = n_o \, \mathcal{L}, \tag{24}$$

where $\mathcal{L} : \Omega \to [0, 1]$ is a windowing mapping that smoothly drives n_o to zero at the extremities.

Denote the elements associated with the state vector of the signal generator as:

$$\theta^\intercal = \begin{bmatrix} 1 & \theta_1 & \theta_2 & \dots & \theta_{2n-1} & \theta_{2n} \end{bmatrix}, \tag{25}$$

where the terms $\theta_{2i-1}(t)$ correspond with cosine functions, while $\theta_{2i}(t)$ are sine functions, for $i \in \{1, \dots, n\}$, and with frequencies $f_{2i-1} = f_{2i} = i\omega_o$. Note that n is the number of frequencies for a given ω_o and ω_{max}. The projection of the tidal elevation onto $\{\theta_i\}$ can be computed as

$$n_o^{\mathcal{L}} \approx L_o \theta, \quad L_o = \langle \theta^\intercal, n_o^{\epsilon} \rangle_\Omega \oslash \langle \theta^\intercal, \oplus_{i=1}^{2n} \theta_i \rangle_\Omega, \tag{26}$$

where the symbol $\oslash$ denotes the standard element-wise (Hadamard) division.

Note that, according to the actual description of n_o, it might not be computationally efficient to use all coefficients from Eq. (26). Instead, the most prominent (in terms of energy) harmonics can be extracted by defining a threshold ϵ such that:

$$\frac{\mathbf{L}_{o,i}^2}{\max_{p \in [1,n]} \{\mathbf{L}_{o,p}^2\}} > \epsilon, \tag{27}$$

where $\mathbf{L}_{o,i}$ is the norm of the coefficients (of the sine and cosine functions) of the ith frequency. This way, the dimension of the signal generator is reduced by eliminating those coefficients below the threshold, with a minor impact on the fidelity of the projection. The resulting signal generator can be defined as:

$$\begin{aligned} & \dot{\theta}_o = S_o \theta_o, \\ & n_o^{\mathcal{L}} \approx L_o \theta_o, \end{aligned} \tag{28}$$

with

$$S_o = 0 \oplus \left(\bigoplus_{p=1}^{j} \begin{bmatrix} 0 & -\omega_p \\ \omega_p & 0 \end{bmatrix} \right), \quad \theta(0) = \mathbf{1}_{2j+1}, \tag{29}$$

and hence

$$\theta_o(t)^\intercal = \begin{bmatrix} 1 & \cos\omega_1 t & \sin\omega_1 t & \dots & \cos\omega_j t & \sin\omega_j t \end{bmatrix}, \tag{30}$$

where $\theta_o(t) \in \mathbb{R}^{2j+1}$ is composed of a certain number of frequencies j, all sharing the same fundamental frequency ω_o. That is to say that the signal generator described by θ_o is used to project $n_o^{\mathcal{L}}$ onto the space

$$\mathcal{X} = \text{span} \left(1 \cup \{\cos\omega_i t, \sin\omega_i t\}_{i \in \mathbb{N}_j} \right). \tag{31}$$

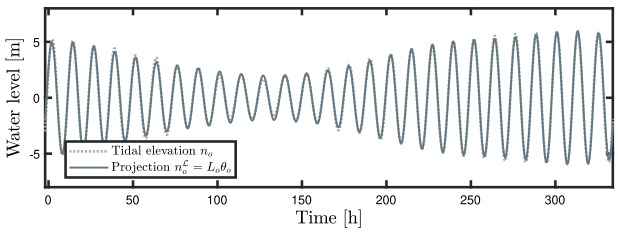

Fig. 6. Representation of the tidal elevation in the moment domain, using the harmonic signal generator θ_o.

Fig. 6 shows the tidal elevation n_o used as input, and its projection onto the harmonic signal generator θ_o, as per Eq. (28). The threshold ϵ is selected to achieve an RMSE between n_o and $n_o^{\mathcal{L}}$ of 0.2 m, which is considered an acceptable approximation of n_o. Note that the RMSE between n_o and its projection, using all coefficients from Eq. (26), tends to zero, since the additional frequencies enhance the approximation of n_o in the moment domain.

3.2.2. Representation of the control inputs in the moment-domain

Eq. (18) computes the steady-state output response of a nonlinear system in terms of the family of continuous functions $\theta(t)$. Nonetheless, while $n_o^{\mathcal{L}}$ can have a certain number of $(j+1)$-components, the manipulated (control) variables can certainly belong to an 'augmented' space, *i.e.* with a larger number of harmonics associated with ω_o (see [23]). To achieve this, an extended higher-dimensional signal generator is defined, with a certain number of harmonics d of each frequency i present in θ_o. First, consider a multiset $\mathcal{F}_o$ such that

$$\mathcal{F}_o = \cup_{p=1}^{d} \{p\omega_i\}_{i \in \mathbb{N}_j}. \tag{32}$$

Note that the multiset $\mathcal{F}_o$ is composed of d multiples of the j frequencies in θ_o. Since all j frequencies share the same fundamental frequency ω_o, by taking multiples of each, $\mathcal{F}_o$ could include each frequency multiple times. Accordingly, the set $\mathcal{F}_c$ is defined as

$$\mathcal{F}_c = \text{set}(\mathcal{F}_o), \tag{33}$$

i.e. as the largest set of elements in $\mathcal{F}_o$ with no repetition of any frequency, and where the maximum frequency is less than, or equal

[1] It can be argued that a set of numbers with a finite number of decimals always share a fractional maximum common divisor, but in our case that leads to a high order signal generator that is not computationally feasible.

to, ω_{max}. Suppose the cardinality of $\mathcal{F}_c$ is $\#\mathcal{F}_c = k \leq d$. Then, the corresponding extended signal generator can be defined as follows:

$$\begin{aligned} \dot{\theta}_c &= S_c \theta_c, \\ Q_t &= L_{Q_t} \theta_c, \\ A_s &= L_{A_s} \theta_c, \end{aligned} \tag{34}$$

with

$$S_c = 0 \oplus \left(\bigoplus_{m=1}^{k} \begin{bmatrix} 0 & \omega_m \\ -\omega_m & 0 \end{bmatrix} \right), \quad \theta_c(0) = \mathbf{1}_{2k+1}, \tag{35}$$

where $\omega_m \in \mathcal{F}_c$, $\forall m \in \mathbb{N}_k$. Note that the tidal elevation can be written in terms of θ_c by simple inclusion, *i.e.* as:

$$n_o^{\mathcal{L}} = [L_o \ \mathbf{0}]\, \theta_c = L_{n_o} \theta_c, \tag{36}$$

where $\mathbf{0}$ is a null vector of appropriate dimensions.

3.2.3. Steady-state output response calculation

To characterise the steady-state response of the tidal barrage system in terms of moments, and then exploit such a parameterisation in the transcription of the OCP in (22), the solution to the differential Eq. (18) must be approximated. Following the procedure outlined in Section 3.1, and considering that the number of harmonics d in the augmented signal generator (34) is sufficiently large, for any given trajectory $\theta_c(t)$, the moment of the tidal barrage system can be approximated [13] as follows:

$$\pi \approx \bar{\pi} = L_{n_i} \theta_c. \tag{37}$$

and hence the steady-state response of the system, corresponding to the system state variable n_i, can be approximated as:

$$n_i^{ss}(t) \approx L_{n_i} \theta_c. \tag{38}$$

L_{n_i} is computed by applying the Galerkin-like method described in Section 3.1. In particular, the state equation corresponding to the hydrodynamics of the barrage system is mapped onto the moment domain by essentially replacing the state and inputs in Eq. (1) with their moment-based parameterisation:

$$A_b L_{n_i} S \theta_c = -L_{Q_t} \theta_c - C_{ds} L_{A_s} \theta_c \sqrt{2g(L_{n_i} - L_{n_o})\theta_c}. \tag{39}$$

For any given L_{n_o}, the corresponding residual map $\mathcal{R}$ can be defined as:

$$\begin{aligned} &\mathcal{R}(L_{n_i}, L_{Q_t}, L_{A_s}, t) = \\ &A_b(L_{n_i}\theta_c(t)) L_{n_i} S \theta_c(t) + L_{Q_t} \theta_c(t) + \\ &C_{ds} L_{A_s} \theta_c(t) \sqrt{2g(L_{n_i} - L_{n_o})\theta_c(t)}. \end{aligned} \tag{40}$$

Finally, the dynamics of the overall barrage system, in the moment-domain, respond to the following non-linear system of equations for a set of N_c collocation instants, *i.e.*

$$R(L_{n_i}, L_{Q_t}, L_{A_s}) = \begin{bmatrix} \mathcal{R}(L_{n_i}, L_{Q_t}, L_{A_s}, t_{N_1}) \\ \vdots \\ \mathcal{R}(L_{n_i}, L_{Q_t}, L_{A_s}, t_{N_c}) \end{bmatrix} = 0. \tag{41}$$

3.2.4. Optimal control problem in the moment domain

Using the parameterisation described in Sections 3.2.1–3.2.3, the optimal control problem (22) can be rewritten as follows:

$$\begin{aligned} &(L_{Q_t^{\text{opt}}}, L_{A_s^{\text{opt}}}) = \\ &\quad \arg \max_{(L_{Q_t}, L_{A_s})} \left[\rho g \int_{\Omega} \mu\, (L_{n_i} - L_{n_o}) \theta_c \left(L_{Q_t} \theta_c \right)^{\mathsf{T}} \mathrm{d}t - C \right], \end{aligned}$$

subject to:

$$\begin{aligned} &R(L_{n_i}, L_{Q_t}, L_{A_s}) = 0, \\ &L_{n_i} \mathcal{A} \leq \mathcal{B}_{n_i}, \\ &L_{Q_t} \mathcal{A} \leq \mathcal{B}_{Q_t}, \\ &L_{A_s} \mathcal{A} \leq \mathcal{B}_{A_s}, \\ &\rho g \mathcal{M} \odot (L_{n_i} - L_{n_o}) \mathcal{A} \odot \left(L_{Q_t} \mathcal{A} \right) \leq \mathcal{B}_{P_t} \end{aligned} \tag{42}$$

Table 2
Parameters from La Rance power plant [14].

Parameter	Value	Unit
Basin surface area $A_b(n_i)$	$0.09336 n_i + 13.1$	km^2
Sluice discharge coefficient C_{ds}	1	–
Turbine discharge coefficient C_{dt}	1	–
Maximum basin level N_i^{max}	5	m
Minimum basin level N_i^{min}	−5	m
Maximum turbine flow Q_t^{max}	280	m^3/s
Number of turbines n_t	24	–
Maximum gate area A_s	900	m^2

Table 3
Descritpion of tidal constituents.

Symbol	Description	Period [h]	Amplitude [m]
M_2	Lunar semidiurnal	12.4206	3.813978
S_2	Solar semidiurnal	12.0000	2.049028
K_1	Lunar diurnal	23.9345	−0.0795165
O_1	Lunar diurnal	25.8193	0.075388

where

$$\begin{aligned} \Lambda &= \left[\theta_c(t_{N_1}) \ \ \ldots \ \ \theta_c(t_{N_c}) \right], \\ \mathcal{A} &= [\Lambda \ \ \Lambda], \\ \mathcal{B}_{n_i} &= \left[n_i^{max} \mathbf{1}_{N_c} \ \ n_i^{min} \mathbf{1}_{N_c} \right], \\ \mathcal{B}_{Q_t} &= \left[Q_t^{max} \mathbf{1}_{N_c} \ \ -Q_t^{max} \mathbf{1}_{N_c} \right], \\ \mathcal{B}_{A_s} &= \left[A_s^{max} \mathbf{1}_{N_c} \ \ \mathbf{0}_{N_c} \right], \\ \mathcal{B}_{P_t} &= \left[P_t^{max} \mathbf{1}_{N_c} \ \ -P_t^{max} \mathbf{1}_{N_c} \right], \end{aligned} \tag{43}$$

$\odot$ denoting the standard element-wise (Hadamard) product and C represented in the moment-domain as:

$$C = k_w L_{A_s} S_c S_c^{\mathsf{T}} L_{A_s}^{\mathsf{T}}. \tag{44}$$

Note that $\mathcal{M}$ is the turbine efficiency mapping μ, which depends on (Q_t, A_s) and is implicitly a function of time, evaluated at the collocation points. In (42), the inequality constraint over P_t is *tightened* by a factor of 10% to ensure that the maximum power is not exceeded, discussed in Section 4.2.

4. Case study and sample results

The tidal barrage model presented in Section 2 is parameterised using the characteristics of the La Rance power plant, as presented in Table 2. Note that the reference value for tidal elevation is the mean sea level; that is, the tidal range has a zero mean, and the basin level is constrained between −5 m and 5 m. The polynomial function describing the basin surface area follows the same convention.

In this study, the four most predominant tidal constituents are used [17]: the principal lunar semidiurnal component M_2, the principal solar semidiurnal component S_2, and the lunar diurnal components K_1 and O_1. Table 3 shows the period and amplitude of each constituent. A tidal elevation forecast of 15 days is extracted from the EDF France website [25], and the amplitudes of each constituent are adjusted to approximately match the forecast with an MSE lower than 0.3 m (which is within the order of uncertainty associated with the forecast itself).

The simulations were performed in MATLAB®, using the non-linear solver `fmincon`, with a timestep of 6 min and a collocation timestep of 30 min. The PC used has a 13th Gen Intel® Core™ i7-1365U processor with 16 GB of RAM. The approximate computational time was of one day for a 14-day window calculation.

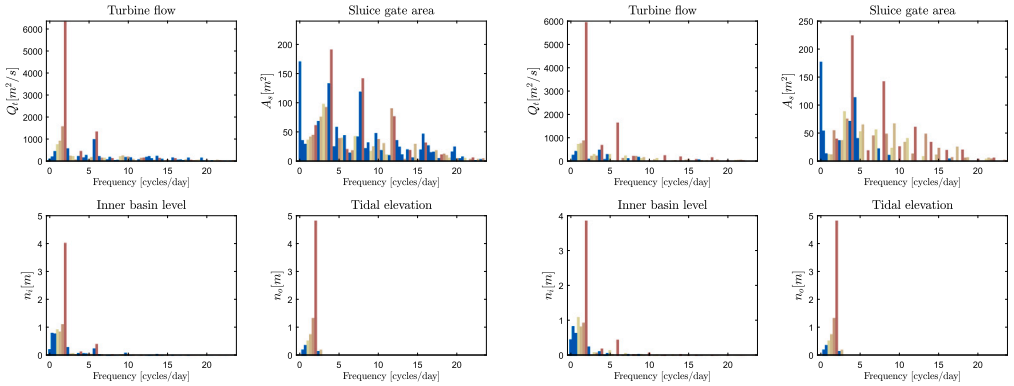

(a) Harmonic expansion of the inputs and outputs of the system using the full spectrum of frequencies.

(b) Harmonic expansion of the inputs and outputs of the system using the parameterisation in terms of θ_c (Eq. (35)).

Fig. 7. Norm of the L coefficients of each frequency for the control (turbine flow Q_t and sluice gate area A_s) and external (tidal elevation n_o) inputs and the output (inner basin level n_i) of the tidal barrage system.

4.1. Harmonic analysis

As described in Section 3.2.2, the representation of the control inputs in the moment domain is assumed to be a harmonic expansion of the frequencies used for the representation of tidal elevation. To evaluate how such a simplifying assumption affects the control solution, a harmonic analysis is performed to determine the dominant frequencies in the solution space.

Initially, the case in which all harmonics n of the corresponding fundamental frequency ω_o are included as part of the corresponding signal generator, until a defined cutoff frequency, is considered. As such, the overall number of harmonics included in the corresponding signal generator is inherently determined by the chosen ω_{max}. For this study, a cutoff frequency of 23 cycles/day (6 radians/day) is adopted to represent the system behaviour. Note that, the longer the time window T_o chosen for the analysis, the smaller the fundamental frequency ω_o, meaning that more harmonics will be needed to reach a given cutoff frequency. In this analysis, a time window of 3 days is chosen, corresponding to a fundamental frequency of 0.33 cycles/day and 70 harmonics.

Fig. 7 shows the resulting frequency domain representation of the tidal elevation, inner basin level, turbine flow and total sluice gate area for this full spectrum case. The four most dominant harmonics in the tidal elevation are coloured in yellow and red, with the remaining harmonics coloured in blue. The darkest red shade corresponds to the semidiurnal component of the tide (close to 2 cycles/day), which is predominant in all three inputs and the system output. It can be seen that harmonics of these four dominant frequencies of the tidal elevation are equally dominant in the turbine flow, sluice gates area and inner basin level, meaning that the controller needs only the most prominent frequencies in the projection of the tide to parameterise the controlled inputs, which is aligned with the proposed parameterisation in Section 3.2.1 (see Eq. (27)). The spectrum of the turbine flow and inner basin level is clearly correlated with the spectrum of the tidal elevation. On the other hand, the spectrum of the sluice gates area covers a wider range of harmonics. Naturally, the constant function {1} (see Eq. (31)) is one of the most predominant, together with harmonics of the semidiurnal component, the dominant one being the double of the semidiurnal component, *i.e.* the sluice gate position operates at double the frequency of the turbine flow. Also, the weight of the harmonics decreases, and can be considered negligible, after 20 cycles/day. The control solution with this parameterisation yields 8 GWh of energy generated.

Now, the same optimisation is run using the parameterisation described in Sections 3.2.1 and 3.2.2, that is, using harmonics of the predominant frequency components of the tidal elevation, as opposed to the full spectrum of frequencies used in the previous case study. In this case, only harmonics of the predominant tidal elevation frequencies are used, resulting in a total of 48 frequencies (30% less compared to the 70 frequencies used in the previous case). The frequency domain representation of the tidal elevation, inner basin level, turbine flow and sluice gates area for this case of reduced number of frequencies is shown in Fig. 7(b).

There is a clear correspondence between the frequencies seen in the solution of the turbine flow control and the inner basin level, in both cases (full spectrum and reduced number of frequencies). The sluice gate control presents more differences between both cases, since the solution in the first case covers the whole spectrum. In the second case, more energy is allocated over a smaller number of frequencies. The energy generated in this second case is 7.34 GWh, 8% lower than in the previous case, which is not negligible. Nonetheless, given that using the full frequency spectrum can be computationally infeasible for longer time simulations, approximating the solution by using harmonics of the tidal elevation frequency is considered appropriate.

4.2. Time-domain simulation results

Fig. 8 shows the results of the optimisation of the turbines flow Q_t and sluice gates area A_s for a neap-spring tidal cycle of 14 days. The operation includes both ebb and flood generation, with pumping. The overall energy generated during the neap-spring cycle (shaving the peak power to the maximum) is 24.4 GWh, which is higher than the average energy produced by the La Rance power plant in 14 days.[2] Note that, in this study, the hill chart used to model the turbines is generic and not the specific hill chart of the turbines from La Rance. Furthermore, the model does not account for the operation of the locks to allow navigation through the barrage, which has an impact on the time windows available for generation. Another source of error in the computation of tidal barrage energy production is the use of a simplified 0D hydrodynamic model, which has been shown in the literature to overestimate energy output, compared to using a 2D hydrodynamic model. For instance, [27] reports that, depending on the operational sequence, the calculated energy output of a proposed project in the Severn Barrage can be up to 10.9% higher with the 0D model than with the 2D model. [14] shows that, in the case of the La Rance power plant, using the 0D model along with the basin topology model (used in

[2] La Rance power plant produces close to 500 GWh per year [26].

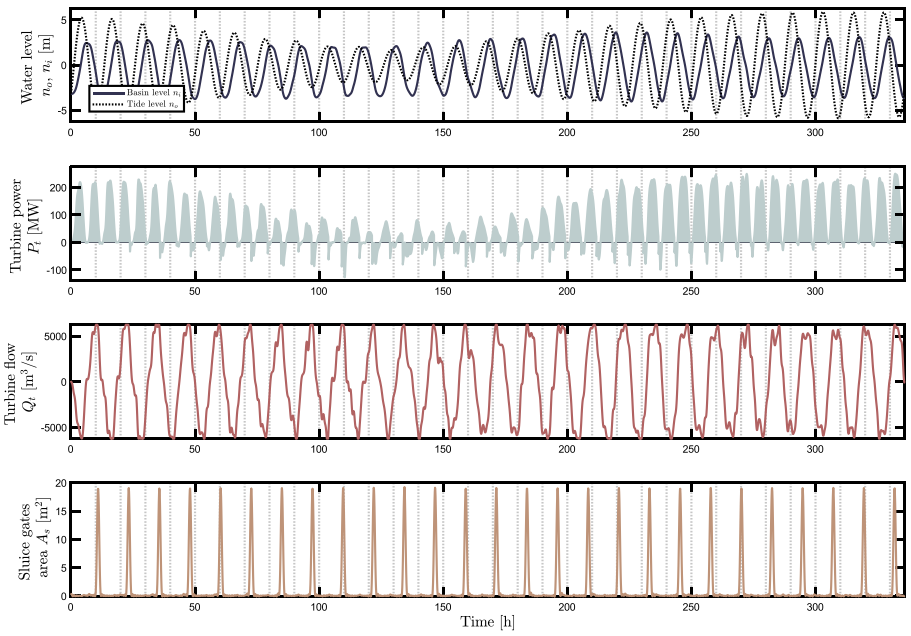

Fig. 8. Optimisation results for a neap-spring cycle (14 days).

this study), the deviation in energy generation is up to 4.7% compared to real measurements.

It is interesting to note that utilisation of the sluice gates is almost negligible compared to the total available area of 900 m^2. One explanation for this is that the model explicitly includes the sluicing operating mode of the turbines. This can potentially be exploited for control co-design of new tidal barrage schemes where the sluicing capacity could be reduced by allocating it to the turbines, leading to saving not only on the investment cost of the tidal barrage but also on operational costs. Nonetheless, the low utilisation of the sluice gates could also be due to misrepresentation of the range of frequencies of the control solution, as seen in Fig. 7. Therefore, the parameterisation of the sluice gates area in the controller may need to include a wider range of frequencies.

One aspect of the control parameterisation to be considered is that, since there is a difference between the real tidal elevation and its representation in the moment domain, the physical system constraints may not be strictly met. This does not happen with the turbine flow, sluice gate area, and basin level constraints, but does happen with the power output constraint; the output power has peaks of up to 4% above the rated power of 240 MW, even after tightening the constraint by 10% to a value of 216 MW. Nonetheless, these peaks appear during very few hours of the time window. If this issue were addressed *a posteriori* by shaving the power peaks to the maximum power of the turbines, the energy output during the complete period of 14 days would decrease by less than 0.1%. In practice, this can be done by manipulating the pitch blades and wicket gates of the turbine in a sub-optimal fashion, to shave some of the hydraulic power.

From Section 2.4.1, the turbine efficiency data is from the manufacturer's data (hill chart) for the type of turbines used at La Rance. In terms of validation, power curves (power P_t vs head H), provided in [14], can be used to compare the power production from the moment-based controller to that currently achievable at La Rance. Fig. 9 shows a significant improvement in the power production capability for the moment-based controller, generally achieving greater power output at each head level, while observing the power capacity limit.

5. Conclusions

This paper presents a detailed model of tidal barrages and its implementation in optimal control of their operation, using the La Rance power plant as study case. The result is a parsimonious representation of the operation of a tidal barrage, which can be parameterised with data from any operating or proposed tidal barrage. The main modelling contribution is on the hydraulic turbine model, for which a generic Andritz Hydro hill chart is used to account for all possible modes of operation, including positive pumping, rarely seen in the literature. One limitation of the model implemented in this study is the use of a simplified 0D model, typical in control studies, to represent the hydrodynamic processes within the barrage basin. As previously mentioned, several studies in the literature show that energy output is overestimated when using a 0D model, compared to using a more accurate 2D hydrodynamic model. It can be argued that, here, the model is used for scheduling rather than for feasibility studies, and that the question is whether the control solution would change if optimising with a 2D model. Because of the computational burden of 2D hydrodynamic models, they are impractical for optimisation purposes, and it remains to be seen if the evaluation of optimal control solutions for tidal barrages is computationally tractable for any models other than 0D models.

On the optimal control problem formulation, using the turbine flow and sluice gates area as manipulated variables accounts for the different operating modes of the barrage in a holistic way, without pre-defining any sequence in the operation and allowing the operation of turbines and sluice gates to be independent from each other. This allows flexibility in the operation; during some cycles, the pumping stages are longer than in others, and generation in one direction can prevail over the other. This flexibility is desirable, given the short-term variability of the tidal range during neap tides compared to spring tides.

Moment-based control appears to be a computationally effective tool to solve the optimal control problem. It solves the control problem in a time window which can include several consecutive cycles, which is essential given the dependence of the available energy during one cycle with the operation during the previous cycle. The mathematical formulation of the moment-based optimal control problem applied to tidal barrage operation is developed considering multiple constituents in the tidal elevation representation, which is a step forward from previous work on this topic.

The frequency analysis shows that only the harmonic expansion of the most prominent frequencies in the tidal elevation are needed to effectively parameterise the control inputs and the output. This drastically decreases the computational burden compared to using the full

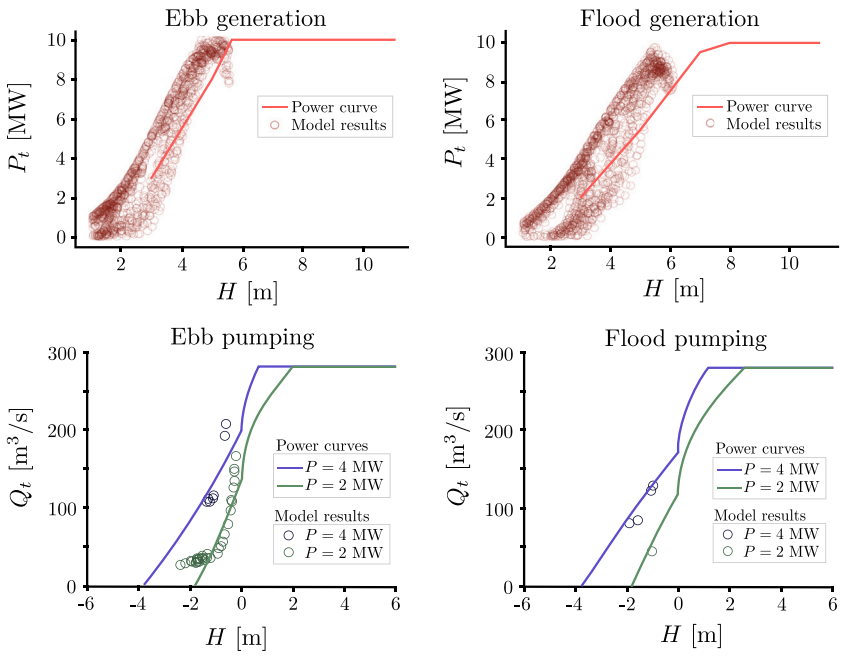

Fig. 9. Turbine power curves (bold lines, adapted from [14]) and model results from simulation (dots).

spectrum of harmonics of the fundamental frequency. However, there is still room to further enhance the performance of the controller in terms of expanding the frequency range. A promising possibility would be to apply receding-horizon control, in which the control problem can be sliced up in more manageable sub-problems, which could improve the optimally of the solution without increasing the computational requirements of the controller.

CRediT authorship contribution statement

Agustina Skiarski: Writing – original draft, Methodology, Formal analysis, Conceptualization. **Nicolás Faedo:** Writing – review & editing, Formal analysis. **John V. Ringwood:** Writing – review & editing, Supervision, Methodology.

Declaration of competing interest

The authors declare that they have no known competing financial interests or personal relationships that could have appeared to influence the work reported in this paper.

Acknowledgements

This work was supported by Taighde Éireann – Research Ireland under Grant number 18/CRT/6049. For the purpose of Open Access, the author has applied a CC BY public copyright licence to any Author Accepted Manuscript version arising from this submission. John Ringwood was supported by Taighde Éireann – Research Ireland through the MaREI Centre for Energy, Climate and Marine under Grant No. 12/RC/2302_P2.

References

[1] G. Aggidis, O. Feather, Tidal range turbines and generation on the Solway Firth, Renew. Energy 43 (2012) 9–17, http://dx.doi.org/10.1016/j.renene.2011.11.045.

[2] A. Lisboa, T. Vieira, L. Guedes, D. Vieira, R. Saldanha, Optimal analytic dispatch for tidal energy generation, Renew. Energy 108 (2017) 371–379, http://dx.doi.org/10.1016/j.renene.2017.02.058.

[3] Y. Shen, P.-O. Nyman, Optimal operation of tidal plants based on nonlinear model predictive control strategy, in: IOP Conference Series: Earth and Environmental Science, IOP Conf. Ser.: Earth Environ. Sci. 687 (1) (2021) 012101, http://dx.doi.org/10.1088/1755-1315/687/1/012101.

[4] A. Skiarski, N. Faedo, J. Ringwood, Tidal barrage operation optimization using moment-based control, in: Proceedings of the European Wave and Tidal Energy Conference, vol. 15, 2023, http://dx.doi.org/10.36688/ewtec-2023-396, URL https://submissions.ewtec.org/proc-ewtec/article/view/396.

[5] A. Angeloudis, S.C. Kramer, A. Avdis, M.D. Piggott, Optimising tidal range power plant operation, Appl. Energy 212 (2018) 680–690, http://dx.doi.org/10.1016/j.apenergy.2017.12.052.

[6] J. Xue, R. Ahmadian, O. Jones, Genetic Algorithm in tidal range schemes' optimisation, Energy 200 (2020) 117496, http://dx.doi.org/10.1016/j.energy.2020.117496.

[7] L. Mackie, D. Coles, M. Piggott, A. Angeloudis, The potential for tidal range energy systems to provide continuous power: A UK case study, J. Mar. Sci. Eng. 8 (10) (2020) 780, http://dx.doi.org/10.3390/jmse8100780.

[8] J. Xue, R. Ahmadian, O. Jones, R.A. Falconer, Design of tidal range energy generation schemes using a Genetic Algorithm model, Appl. Energy 286 (2021) 116506, http://dx.doi.org/10.1016/j.apenergy.2021.116506.

[9] E.A. Kontoleontos, S. Weissenberger, Annual energy production maximization for tidal power plants with evolutionary algorithms, Int. J. Fluid Mach. Syst. 10 (2017) 264–273, URL https://api.semanticscholar.org/CorpusID:116680863.

[10] J.V. Ringwood, N. Faedo, Tidal barrage operational optimisation using wave energy control techniques, in: Proceedings of the 14th IFAC Conference on Control Applications in Marine Systems, Robotics, and Vehicles CAMS 2022, vol. 55, (31) Elsevier BV, Lyngby, Denmark, 2022, pp. 148–153, http://dx.doi.org/10.1016/j.ifacol.2022.10.423.

[11] A. Astolfi, Model Reduction by Moment Matching for Linear and Nonlinear Systems, vol. 55, IEEE, 2010.

[12] N. Faedo, G. Scarciotti, A. Astolfi, J.V. Ringwood, Energy-maximising control of wave energy converters using a moment-domain representation, Control Eng. Pract. 81 (2018) 85–96, http://dx.doi.org/10.1016/j.conengprac.2018.08.010, URL https://www.sciencedirect.com/science/article/pii/S0967066118304246.

[13] N. Faedo, G. Scarciotti, A. Astolfi, J.V. Ringwood, On the Approximation of Moments for Nonlinear Systems, Tech. Rep., 11, IEEE, 2021, pp. 5538–5545, http://dx.doi.org/10.1109/TAC.2021.3054325.

[14] T.M. Moreira, J.G. de Faria, P.O.V. de Melo, G. Medeiros-Ribeiro, Development and validation of an AI-driven model for the La Rance tidal barrage: A generalisable case study, Appl. Energy 332 (2023) 120506, http://dx.doi.org/10.1016/j.apenergy.2022.120506.

[15] N. Yates, I. Walkington, R. Burrows, J. Wolf, The energy gains realisable through pumping for tidal range energy schemes, Renew. Energy 58 (2013) 79–84, http://dx.doi.org/10.1016/j.renene.2013.01.039.

[16] A. Angeloudis, M. Piggott, S. Kramer, A. Avdis, D. Coles, M. Christou, Comparison of 0-D, 1-D and 2-D model capabilities for tidal range energy resource assessments, in: Proceedings of the Twelfth European Wave and Tidal Energy Conference, Cork, Ireland, 2017.

[17] B.B. Parker, Tidal Analysis and Prediction, in: NOAA Special Publication NOS CO-OPS, U.S. Department of Commerce, National Oceanic and Atmospheric Administration, National Ocean Service, Center for Operational Oceanographic Products and Services, 2007.

[18] S. Waters, G. Aggidis, Tidal range technologies and state of the art in review, Renew. Sustain. Energy Rev. 59 (2016) 514–529, http://dx.doi.org/10.1016/j.rser.2015.12.347.

[19] C. Yang, Y. Zheng, D. Zhou, X. Ge, L. Li, Bidirectional power performance of a tidal unit with unilateral and double guide vanes, Adv. Mech. Eng. 5 (2013) 415–427, http://dx.doi.org/10.1155/2013/835051.

[20] G.A. Aggidis, A. Židonis, Hydro turbine prototype testing and generation of performance curves: Fully automated approach, Renew. Energy 71 (2014) 433–441, http://dx.doi.org/10.1016/j.renene.2014.05.043.

[21] G.V. Cybenko, Approximation by superpositions of a sigmoidal function, Math. Control Signals Systems 2 (1989) 303–314, URL https://api.semanticscholar.org/CorpusID:3958369.

[22] M. Hagan, H. Demuth, M. Beale, Neural Network Design, PWS Publishing, Boston, MA, 1996.

[23] N. Faedo., G. Scarciotti., A. Astolfi., J.V. Ringwood, Nonlinear energy-maximizing optimal control of wave energy systems: A moment-based approach, IEEE Trans. Control Syst. Technol. 29 (6) (2021) 2533–2547, http://dx.doi.org/10.1109/TCST.2020.3047229.

[24] N. Faedo, Y. Peña-Sanchez, J.V. Ringwood, Receding-horizon energy-maximising optimal control of wave energy systems based on moments, IEEE Trans. Sustain. Energy 12 (1) (2020) 378–386.

[25] E. France, Marées en Rance, 2024, URL https://www.edf.fr/usine-maremotrice-rance/marees-en-rance, (Accessed March 2024).

[26] E. France, L'usine marémotrice de la Rance, 2024, URL https://www.edf.fr/usine-maremotrice-rance, (Accessed March 2024).

[27] F. Harcourt, A. Angeloudis, M.D. Piggott, Utilising the flexible generation potential of tidal range power plants to optimise economic value, Appl. Energy 237 (2019) 873–884, http://dx.doi.org/10.1016/j.apenergy.2018.12.091.